Electronic Supplementary Information

Stable organic lead iodides with three-dimensional crystallographic and electronic structures showing high photoresponse

Chang-Chun Fan[a], Bei-Dou Liang[a], Cheng-Dong Liu[a], Chao-Yang Chai[a], Xiang-Bin Han[a]*, Wen Zhang[a]*

[a]Jiangsu Key Laboratory for Science and Applications of Molecular Ferroelectrics and School of Chemistry and Chemical Engineering, Southeast University, Nanjing 211189, China

Experimental

Fig. S1. PXRD patterns.

Fig. S2. The bandgap is deduced from the Tauc equation.

Fig. S3. Semiconducting properties of (Mpda)Pb_2I_6.

Fig. S4. Edge-sharing "Step-like" connection in the (110) direction.

Fig. S5. Structural properties (M_2da)Pb_2I_6.

Fig. S6 Structural property in (Mpda)Pb_2I_6.

Fig. S7. (a) Cation and (b-d) N−H···halogen and C−H···halogen interactions between the organic cations and inorganic layers of (M_2pda)Pb_2I_6 at 100 K.

Fig. S8. (a) Hirshfeld surface and (b-d) 2D fingerprint plots of (M_2pda)Pb_2I_6 at 100 K.

Fig. S9. Difference of bond angle below (a) and above (b) the phase transition of (M_2pda)Pb_2I_6.

Fig. S10. Structural distortions of the inorganic sublattice in (M_2pda)Pb_2I_6 at 100 K (a and b) and 298 K (c and d).

Fig. S11. Dielectric transition of (H_2bda)Pb_2I_6 at different frequencies.

Fig. S12. (a) Hirshfeld surface and (b-d) 2D fingerprint plots of (H_2bda)Pb_2I_6 at 100 K.

Fig. S13. Photographs of crystal at 298 K and 40% relative humidity at t = 0 hours (left), t = 14 hours (middle) and t = 20 hours (right).

Fig. S14. Possible decomposition pathway of lead halide perovskites in the presence of water.

Fig. S15.Steady-state photocurrent under 120 mW/cm^2 sunlight illumination.

Table S1. Crystallographic data and refinement parameters for $(M_2pda)Pb_2I_6$, $(Mpda)Pb_2I_6$ and $(H_2bda)Pb_2I_6$.

Table S2. Selected hydrogen bonds for$(M_2pda)Pb_2I_6$ (100 K) and $(H_2bda)Pb_2I_6$ (298 K).

Table S3. Bond angles and bond lengths of $(M_2pda)Pb_2I_6$, $(Mpda)Pb_2I_6$ and $(H_2bda)Pb_2I_6$.

Table S4. Survey of intra-octahedral distortions in $(M_2pda)Pb_2I_6$.

Table S5. Structure optimization for DFT calculation.

Experimental

Materials and general characterizations. All reagents were commercially available and used as received without further purification. Powder X-ray diffraction (PXRD) patterns were obtained on a Rigaku SmartLab X-ray diffraction instrument. Differential scanning calorimetry measurement was carried out on a TA Instrument SDT-Q10 at a scanning rate of 10 K min^{-1} under nitrogen. Thermogravimetric analysis (TGA) was performed by a NETZSCH TG209 F3 system. Temperature-dependent dielectric constant spectra were measured on powdered and single-crystal samples by using a Tonghui TH2828A impedance analyzer at frequencies of 1−1000 kHz with an applied electric field of 1 V. Ultraviolet-vis (UV-vis) absorption spectra were measured with Shimadzu UV-2600 equipped with ISR-2600Plus integrating sphere.

Synthesis of the titled compound. $Pb(AcO)_2$ (15 mmol) was dissolved in HI solution (60 mL) at 130 °C, followed by addition of 1 mL of 50% H_3PO_2 solution and M_2pda (5 mmol). Yellow precipitates appeared and then were dissolved by stirring. The resulting solution was evaporated at 60 °C. Millimeter-sized red block-shaped crystals were obtained with a yield of about 80%. Phase purity for batches of crystalline samples was confirmed by PXRD (Fig. S1). Other titled compounds are the same.

Synthesis of $MAPbI_3$. $Pb(AcO)_2$ (12.6 mmol) and MAI (12.6 mmol) were dissolved in HI solution (40 mL) at 60 °C, followed by addition of 1 mL of 50% H_3PO_2 solution . The resulting yellow solution was evaporated at 60 °C. Black block-shaped crystals were obtained.

Synthesis of $MAPbI_3$. $Pb(AcO)_2$ (12.6 mmol) and MAI (12.6 mmol) were dissolved in gamma-butyrolactone (40 mL) at 60 °C. The resulting yellow solution was evaporated at 60 °C. Millimeter-sized black block-shaped crystals were obtained.

Single-crystal X-ray Diffraction. Crystallographic data were collected on a Rigaku Oxford Diffraction Supernova Dual Source, Cu at Zero equipped with an AtlasS2 CCD using Mo Kα radiation. CrysAlisPro 1.171.40.84a (Rigaku OD, 2020) was used to collect data, refine cells, and reduce data. SHELXL-2018 package was used to solve the structures by direct methods. All non-hydrogen atoms were refined anisotropically. The details of crystal data are given in Tables S1 and S2. CCDC 2183780-2183783 contain the crystallographic data for $(M_2pda)Pb_2I_6$, $(Mpda)Pb_2I_6$, and $(H_2pda)Pb_2I_6$. These data can be

obtained free of charge via http://www.ccdc.cam.ac.uk/conts/retrieving.html, or from the Cambridge Crystallographic Data Centre, 12 Union Road, Cambridge CB2 1EZ, UK; fax: +44 1223-336-033; or e-mail: deposit@ccdc.cam.ac.uk.

***I-V* measurement.** Simulated AM 1.5 G irradiation was produced by a CEL-S500/350 solar simulator (Ceaulight, 350 W) with an AM1.5 filter. The light intensity was measured and calibrated by a Si photodetector connected with a power meter (CEL-NP2000-2A, Ceaulight). *I-V* measurements were performed by a PDA FS380 Source meter under AM 1.5 G illumination.

Theoretical calculations. DFT calculations were conducted by using the Vienna ab initio simulation package.[1] The projector augmented wave method was adopted to define the ion-electron interactions.[2] The exchange-correlation interaction was expressed by the Perdew–Burke–Ernzerhof (PBE) functional within the generalized gradient approximation.[3] Grimme's dispersion-corrected semi-empirical DFT-D3 method was employed to evaluate van der Waals interactions, affording optimized lattice parameters comparable to the experimental results (Table S5).[4] The energy cutoff was set to 500 eV and a 4×2×5 Monkhorst-Pack grid of k-points was used.[5] VASPKIT was employed to perform post-processing analysis.[6]

References

1. Kresse, G.; Furthmüller, J. Efficient iterative schemes for ab initio total-energy calculations using a plane-wave basis set. *Phys. Rev. B.* **1996**, 54, 11169-11186.
2. Blöchl, P. E.; Projector augmented-wave method. *Phys. Rev. B.* **1994**, 50, 17953-17979.
3. Perdew, J. P.; Burke, K.; Ernzerhof, M. Generalized gradient approximation made simple. *Phys. Rev. Lett.* **1996**, 77, 3865-3868.
4. Grimme, S.; Antony, J.; Ehrlich, S.; Krieg, H. *J. Chem. Phys.* **2010**, 132, 154104.
5. Monkhorst, H. J.; Pack, J. D. Special points for Brillouin-zone integrations. *Phys. Rev. B.* **1976**, 13, 5188-5192.
6. Wang, V.; Xu, N.; Liu, J. C.; Tang, G.; Geng, W. T. VASPKIT: A user-friendly interface facilitating high-throughput computing and analysis using VASP code. *Comput. Phys. Commun.* **2021**, 267, 108033.

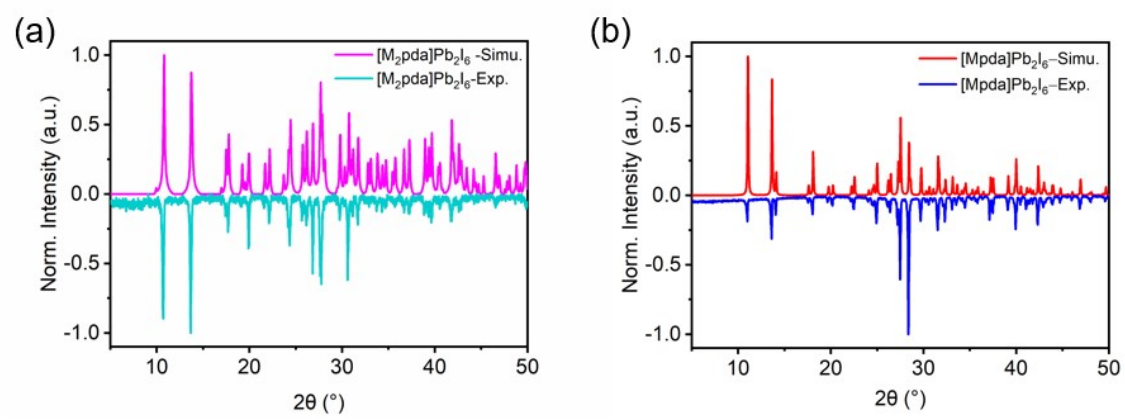

Fig. S1. PXRD patterns of (a) $(M_2pda)Pb_2I_6$; (b) $(Mpda)Pb_2I_6$.

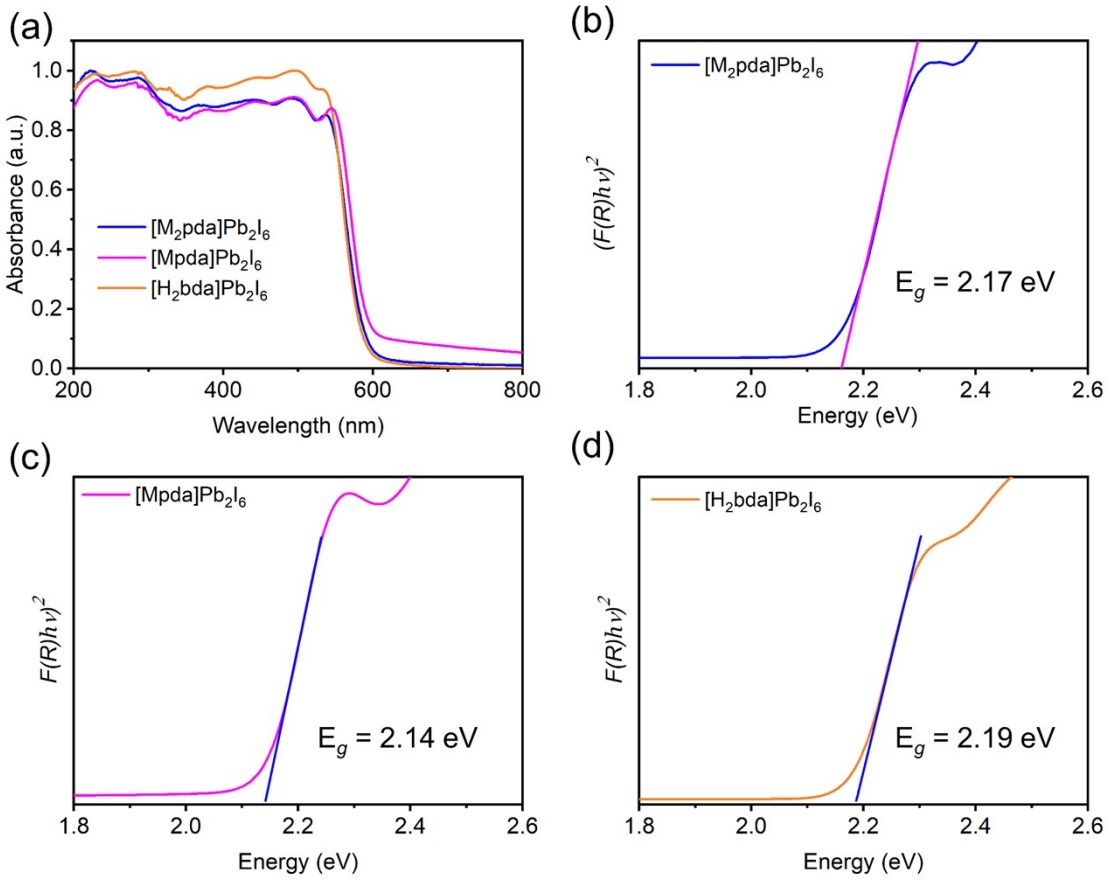

Fig. S2. (a) UV−vis absorption spectrum of $(M_2pda)Pb_2I_6$, $(Mpda)Pb_2I_6$, and $(H_2pda)Pb_2I_6$. (b-d) The bandgap is deduced from the Tauc equation.

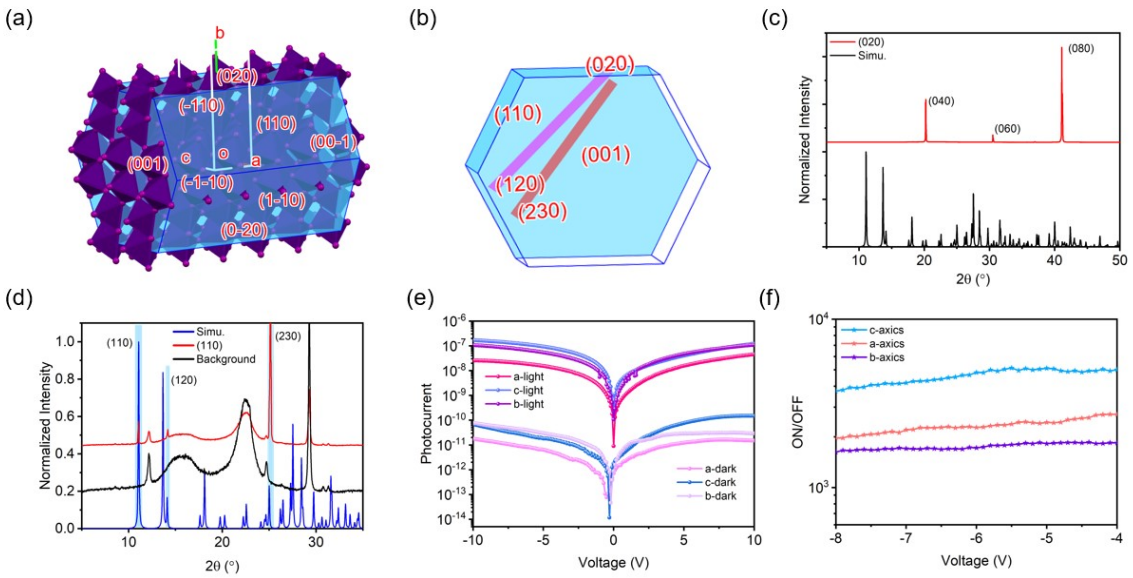

Fig. S3. Semiconducting properties of (Mpda)Pb_2I_6. (a, b) The calculated crystal morphology in Mercury; (c, d) PXRD patterns of a single crystal recorded from the (020) plane and (110); (e, f) Isotropic photoresponse measured along different axis directions.

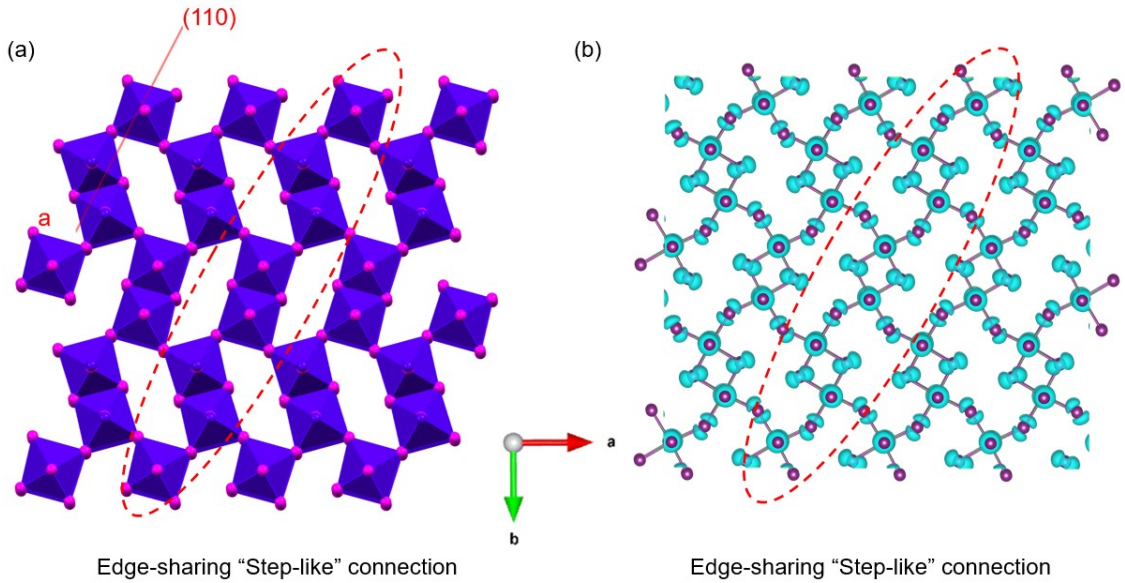

Fig. S4. Edge-sharing “Step-like” connection in the (110) direction. (a) The inorganic framework edge-sharing “step-like” connection in the (110) direction. (b) Isosurface plots of charge density corresponding to CBM at the Z point in the (110) direction.

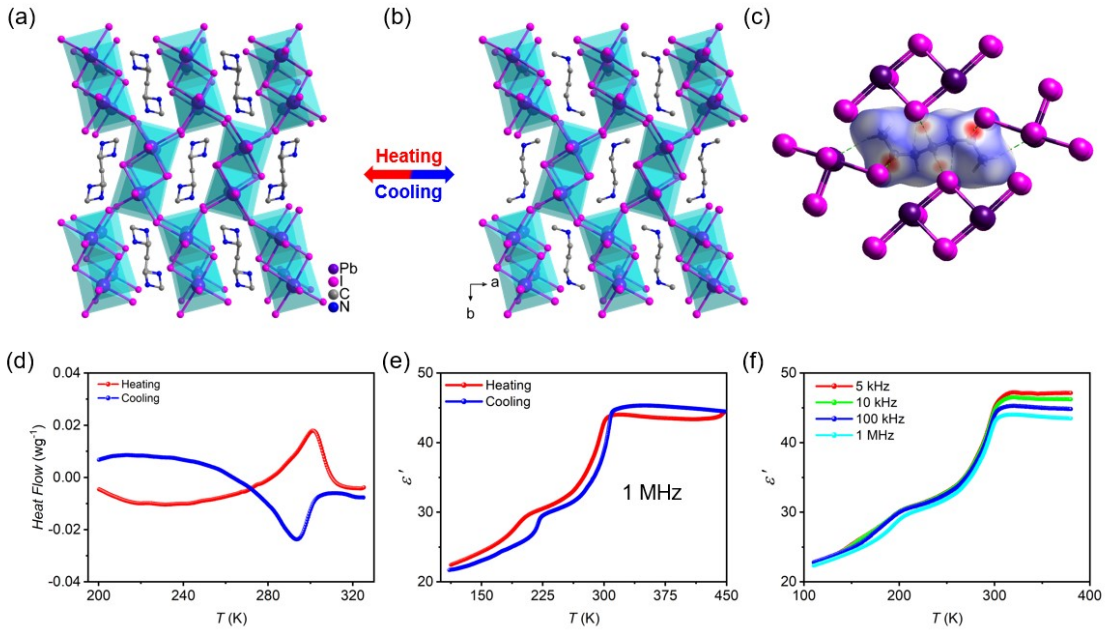

Fig. S5. Structural properties of $(M_2pda)Pb_2I_6$: (a, b) Disorder and order states of $(M_2pda)^{2+}$ cations at 298 and 100 K. Disordered atoms and H atoms are omitted for clarity; (c) Hirshfeld surface at 100 K; (d) DSC curves; (e) Dielectric transition; (f) Dielectric transition at different frequencies.

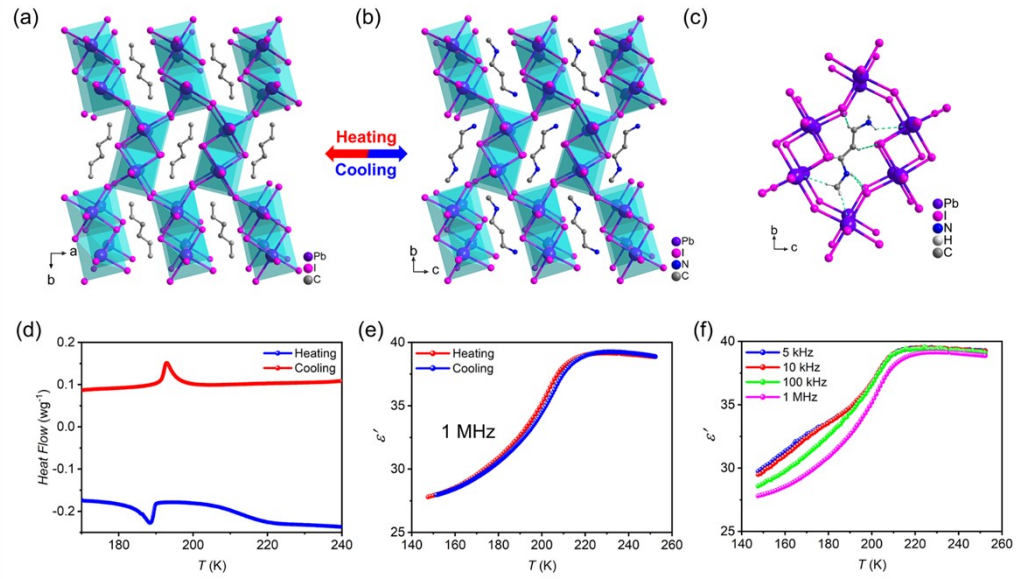

Fig. S6. Structurpropertiesies in $(Mpda)Pb_2I_6$: (a, b) Disorder and order state of cations of $(Mpda)^{2+}$ at 298 and 100 K. Disordered atoms and H atoms are omitted for clarity; (c) 3D dnorm surface of $(M_2pda)Pb_2I_6$ at 100 K; (d) DSC curves; (e) Dielectric transition; (f) Dielectric transition at different frequencies.

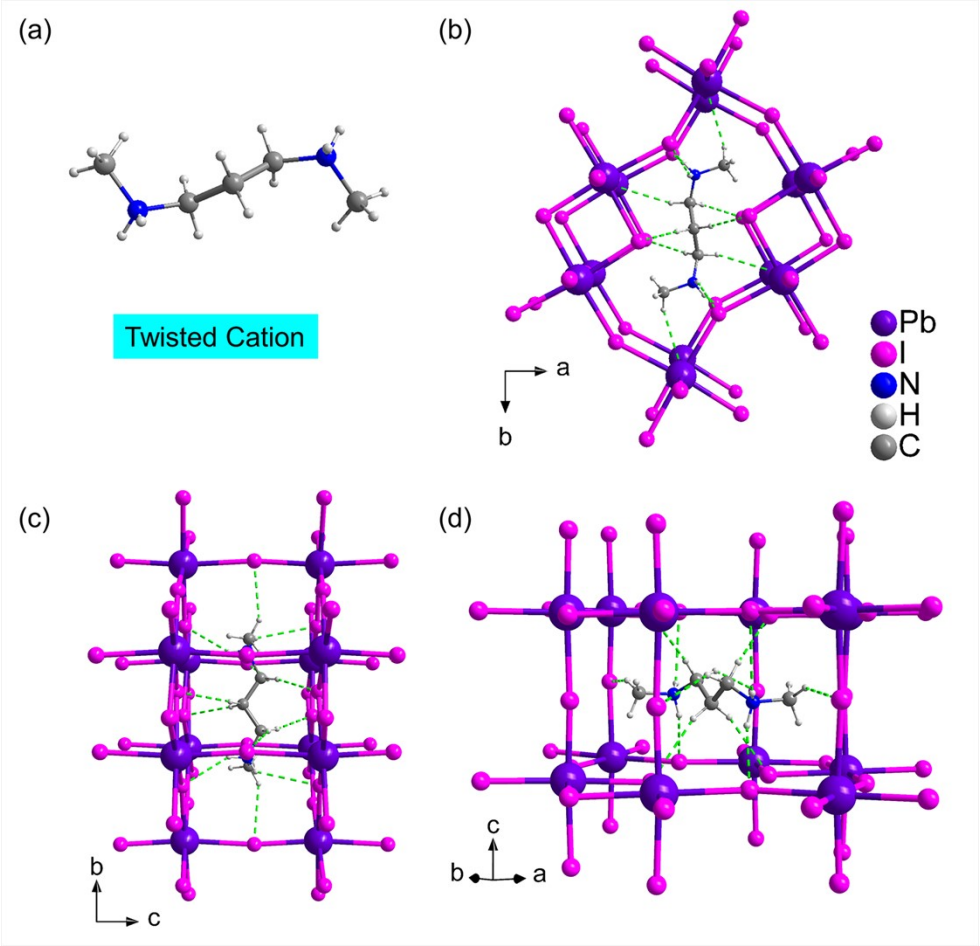

Fig. S7. (a) twisted cation; (b-d) N−H···halogen and C−H···halogen interactions between the organic cations and inorganic layers of $(M_2pda)Pb_2I_6$ at 100 K.

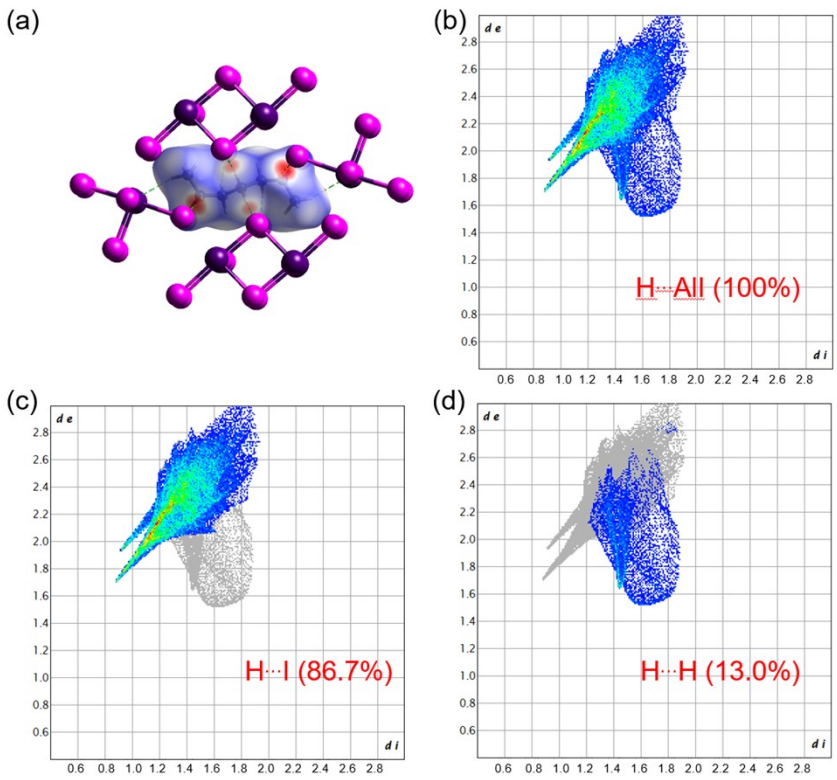

Fig. S8. (a) Hirshfeld surface and (b-d) 2D fingerprint plots of $(M_2pda)Pb_2I_6$ at 100 K. Red, white and blue regions of the Hirshfeld surfaces indicate positive (close contact), neutral and negative isoenergies, respectively. In the plot, the d_i and d_e denote the distances from the surface to the nearest atom interior and exterior to the surface, respectively.

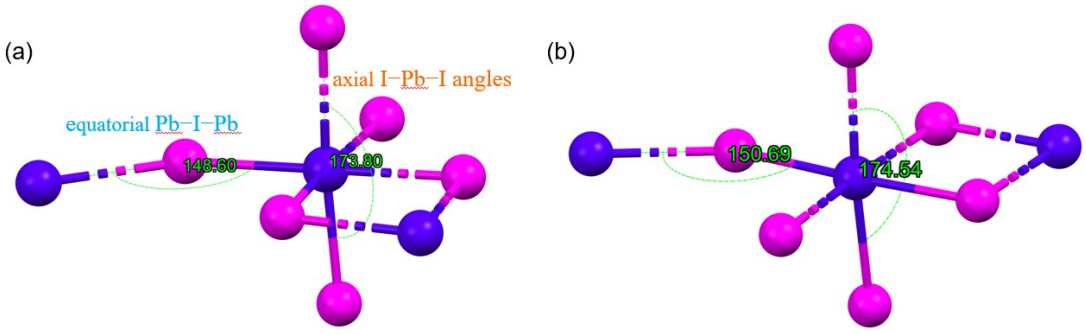

Fig. S9. The difference of bond angles before (a, LTP) and after (b, HTP) the phase transition of $(M_2pda)Pb_2I_6$.

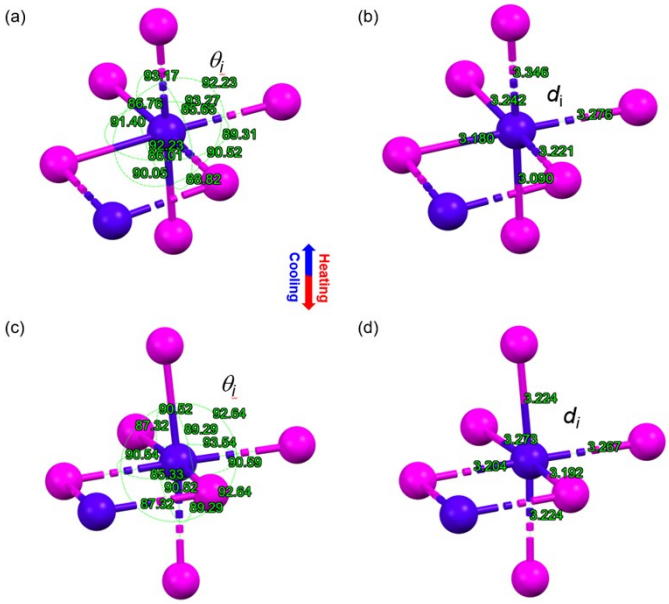

Fig. S10. Structural distortions of the inorganic sublattice in $(M_2pda)Pb_2I_6$ at 100 K (a, b) and 298 K (c, d), (a, c) I−Pb−I bond angles (θ_i), and (b, d) Pb−I bond lengths (d_i).

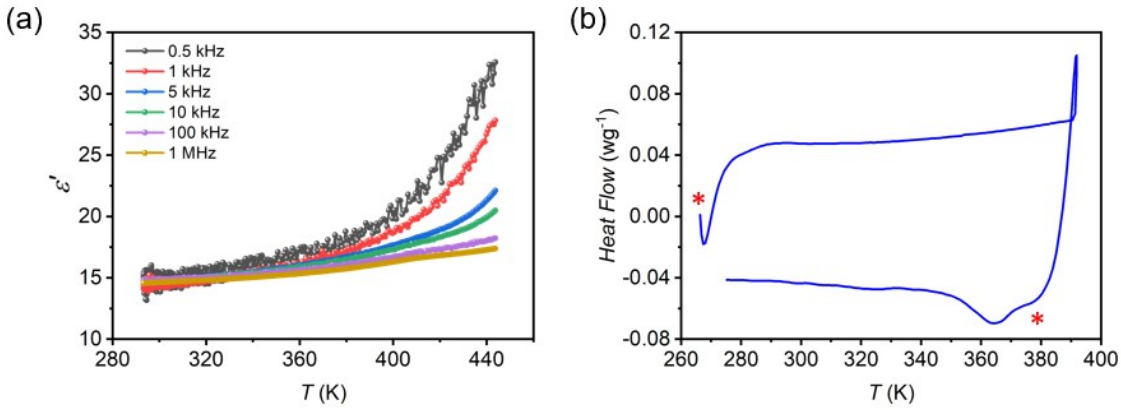

Fig. S11. (a) Dielectric transition of $(H_2bda)Pb_2I_6$ at different frequencies; (b) DSC curve of $(H_2bda)Pb_2I_6$ (* represents the start-up signals instead of the signal from samples). Dielectric and DSC experiments show that $(H_2pda)Pb_2I_6$ does not undergo structural phase transition below 400 K.

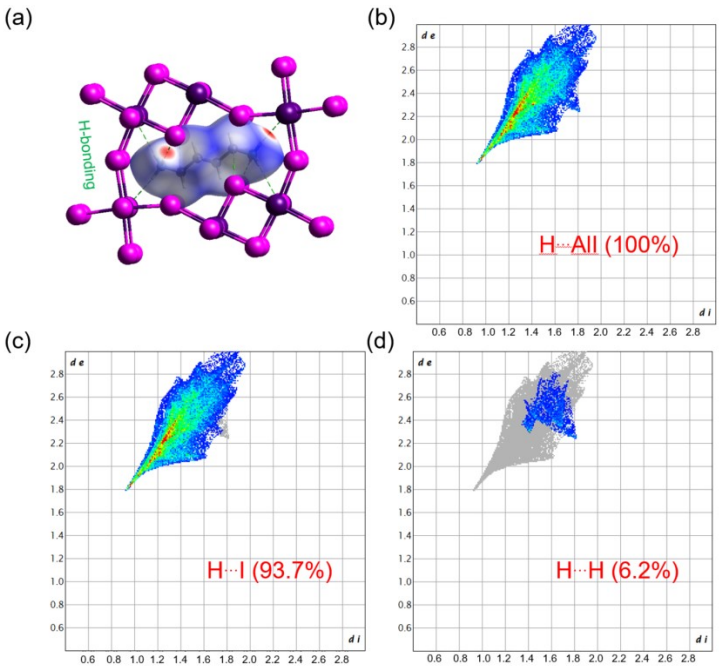

Fig. S12. (a) Hirshfeld surface and (b-d) 2D fingerprint plots of $(H_2bda)Pb_2I_6$ at 298 K. Red, white and blue regions of the Hirshfeld surfaces indicate positive (close contact), neutral and negative isoenergies, respectively. In the plot, the d_i and d_e denote the distances from the surface to the nearest atom interior and exterior to the surface, respectively.

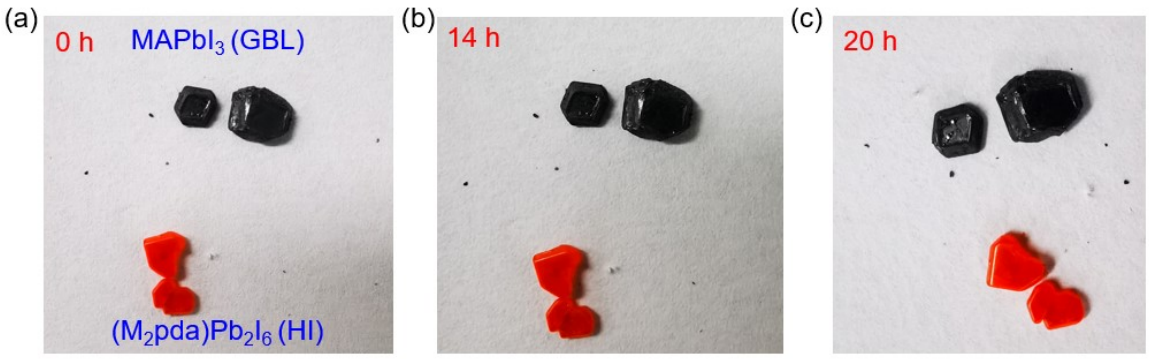

Fig. S13. Photographs of crystal at 298 K and 40% relative humidity at t = 0 hours (left), t = 14 hours (middle) and t = 20 hours (right).

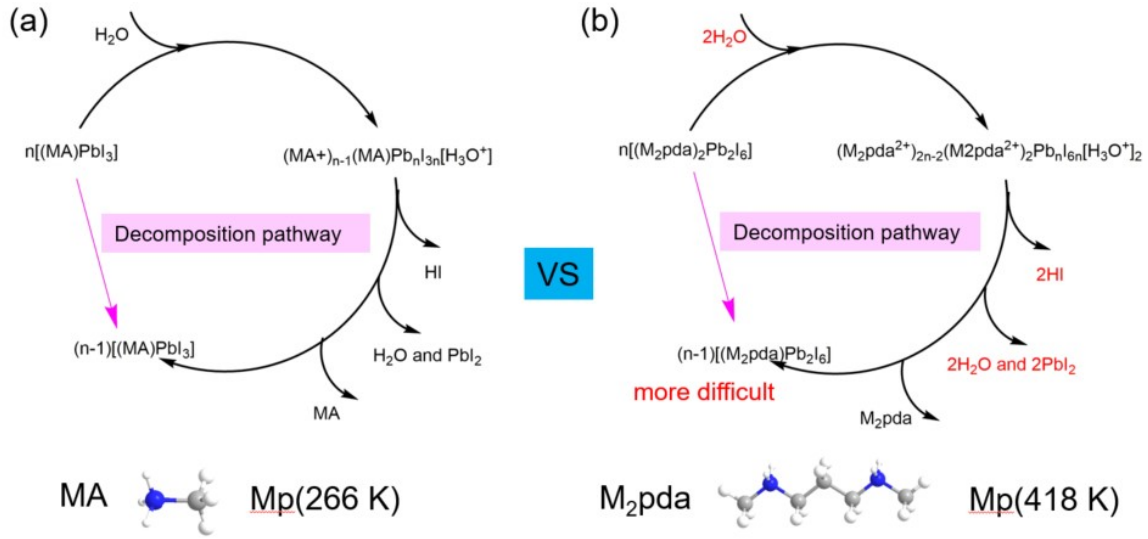

Fig. S14. Possible decomposition pathway of lead halide perovskites in the presence of water: (a) Decomposition pathway of $MAPbI_3$; (b) Decomposition pathway of $(M_2pda)Pb_2I_6$.

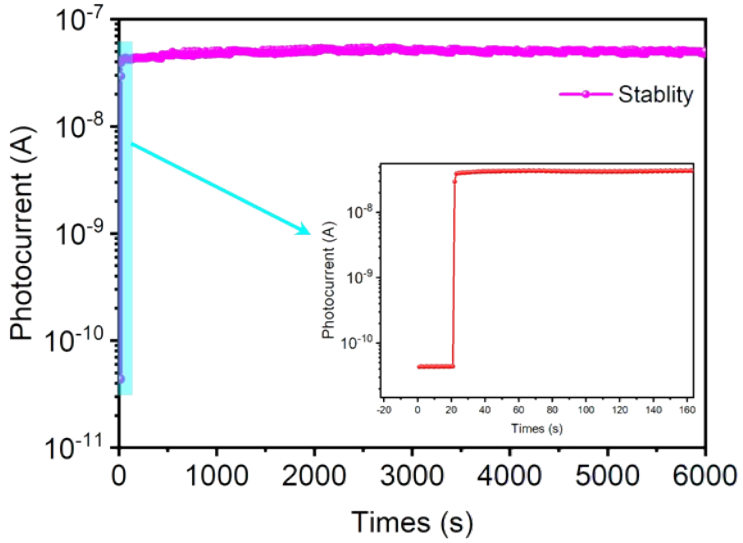

Fig. S15. Steady-state photocurrent under 120 mW/cm^2 sunlight illumination.

Table S1. Crystallographic data and refinement parameters for $(M_2pda)Pb_2I_6$, $(Mpda)Pb_2I_6$, and $(H_2bda)Pb_2I_6$.

	$[M_2pda]Pb_2I_6$		$[Mpda]Pb_2I_6$	$[H_2bda]Pb_2I_6$
	100 K	298 K	298K	298K
Formula	$C_5H_{16}N_2Pb_2I_6$	$C_5H_{16}N_2Pb_2I_6$	$C_4H_{14}N_2Pb_2I_6$	$C_4H_{14}N_2Pb_2I_6$
Formula weight	1279.98	1279.98	1265.95	1265.95
Crystal system	Orthorhombic	Orthorhombic	Orthorhombic	Monoclinic
space group	$P2_12_12$	*Pbam*	*Pbam*	$P2_1/c$
a / Å	9.1348(10)	9.2222(5)	8.9733(9)	6.5066(5)
b / Å	17.6663(19)	17.7717 (7)	17.5285 (11)	17.0103(14)
c / Å	6.4266(10)	6.4398(3)	6.4748(6)	9.2072(7)
α / º	90	90	90	90
β / º	90	90	90	92.815(7)
γ / º	90	90	90	90
V / Å^3	1037.1(2)	1055.45 (9)	1018.41 (14)	1017.82(14)
Z	2	2	2	2
Flack parameter	0.48(17)	/	/	/
D_{calc} / g·cm^{-3}	4.099	4.017	4.082	4.131
μ / mm^{-1}	25.125	24.688	25.582	25.599
total reflns	2249	1395	1340	2504
obsd reflns (I > 2σ(I))	1964	1140	945	1678
R_{int}	0.031	0.040	0.035	0.0554
R_1[a] /wR_2[b] (I > 2σ(I))	0.0712, 0.1379	0.0508, 0.1230	0.0364, 0.0787	0.0411, 0.0879
R^1/wR^2 (all data)	0.0802, 0.1442	0.0612, 0.1273	0.0646, 0.0873	0.0737, 0.0994
GOF	1.11	1.066	1.044	1.099
$\Delta\rho$[c] / e·Å^{-3}	6.42/−4.44	1.66/−3.35	1.29/−1.06	1.34/−2.28

[a] $R_1 = \Sigma| |F_o| - |F_c| | / |F_o|$. [b] $wR_2 = [\Sigma w(F_o^2-F_c^2)^2] / \Sigma w(F_o^2)^2]^{1/2}$. [c] Maximum and minimum residual electron density.

Table S2. Selected hydrogen bonds for $(M_2pda)Pb_2I_6$ (100 K) and $(H_2bda)Pb_2I_6$ (298 K).

D−H···A	D−H / Å	H···A / Å	D···A / Å	∠DHA / °
$(M_2pda)Pb_2I_6$				
N(1)−H(1B)···I(3)^{i}	0.91	3.10	3.77(5)	132.1
N(1)−H(1A)···I(3)^{ii}	0.91	2.65	3.46(5)	141.9
Symmetry codes: (i) *x*−1/2, −*y*+3/2, −*z*; (ii) *x*−1/2, −*y*+3/2, −*z*+1.				
$[H_2bda]Pb_2I_6$				
N(1)−H(1E)···I(1)^{i}	0.89	2.90	3.764(12)	164.8
N(1)−H(1D)···I(3)^{ii}	0.89	2.84	3.687(14)	160.1
N(1)−H(1C)···I(3)^{iii}	0.89	3.04	3.767(11)	140.1
C(2)−H(2B)···I(2)^{iv}	0.97	3.26	4.024(14)	137.3
C(2)−H(2B)···I(1)^{v}	0.97	3.14	3.811(15)	127.9
C(2)−H(2A)···I(2)	0.97	3.30	3.939(15)	125.1
C(1)−H(1A)···I(1)^{i}	0.97	3.17	3.805(11)	124.7
Symmetry codes: (i) −x+1, −y+1, −z+1; (ii) x−1, −y+1/2, z−1/2; (iii) x−1, y, z−1; (iv) x−1, y, z; (v) −x, −y+1, −z+1.				

Table S3. Bond angles and bond lengths of $(M_2pda)Pb_2I_6$, $(Mpda)Pb_2I_6$, and $(H_2bda)Pb_2I_6$.

Bond angles	Angle / °	Bond lengths	Length / Å
$(M_2pda)Pb_2I_6$-100K			
Pb(1)–I(1)–Pb(1)^{i}	93.89(6)	Pb(1)–I(1)	3.180(2)
Pb(1)–I(2)–Pb(1)^{iV}	173.80(10)	Pb(1)–I(2)^{i}	3.221(2)
Pb(1)–I(3)–Pb(1)^{V}	148.62(8)	Pb(1)–I(2)	3.346(3)
I(2)– Pb(1)–I(1)	90.07(7)	Pb(1)–I(2)^{ii}	3.090(3)
I(2)– Pb(1)–I(1)^{i}	88.84(8)	Pb(1)–I(3)	3.242(2)
I(1)– Pb(1)–I(1)^{i}	86.00(7)	Pb(1)–I(3)^{iii}	3.275(2)
I(2)– Pb(1)–I(3)	92.20(9)		
I(1)– Pb(1)–I(3)	91.39(6)		
I(1)^{i}– Pb(1)–I(3)	177.20(7)		
I(2)– Pb(1)–I(3)^{ii}	90.54(8)		
I(1)– Pb(1)–I(3)^{ii}	175.27(6)		
I(1)^{i}– Pb(1)–I(3)^{ii}	89.32(6)		
I(3)– Pb(1)–I(3)^{ii}	93.27(4)		
I(2)– Pb(1)–I(2)^{iii}	173.80(10)		
I(1)– Pb(1)–I(2)^{iii}	86.73(7)		
I(1)^{i}– Pb(1)–I(2)^{ii}	85.64(7)		
I(3)– Pb(1)–I(2)^{iii}	93.19(8)		
I(3)^{ii}– Pb(1)–I(2)^{iii}	92.22(8)		
Symmetry codes:(i): 1+x, +y, 1+Z; (ii) 1–x, 1/2+y, 1–Z; (iii) 1–x, –1/2+y, 1–z; (iv) –1+x, +y, –1+z.			
$(M_2pda)Pb_2I_6$-298K			
Pb(1)–I(1)–Pb(1)^{i}	94.68(3)	Pb(1)–I(1)	3.1923(10)
Pb(1)–I(2)–Pb(1)^{iV}	174.55(4)	Pb(1)–I(2)^{i}	3.2043(9)
Pb(1)–I(3)–Pb(1)^{V}	150.69(4)	Pb(1)–I(2)	3.22355(16)
I(1)^{i}–Pb(1)–I(3)^{iii}	175.92(3)	Pb(1)–I(2)^{ii}	3.22355(16)
I(1)^{i}–Pb(1)–I(3)	90.54(3)	Pb(1)–I(3)^{iii}	3.2668(10)
I(1)– Pb(1)–I(1)^{i}	85.33(3)	Pb(1)–I(3)	3.2730(10)
I(2)^{ii}–Pb(1)–I(2)	174.55(4)		
I(1)–Pb(1)–I(3)^{iii}	90.60(3)		
I(1)– Pb(1)–I(3)	175.86(3)		
I(2)–Pb(1)–I(3)^{iii}	92.64(2)		
I(2)–Pb(1)–I(3)	90.52(2)		
I(1)–Pb(1)–I(2)^{ii}	89.29(2)		
I(1)–Pb(1)–I(2)	89.29 (2)		
I(2)–Pb(1)–I(3)^{iii}	92.64(2)		
I(1)^{i}–Pb(1)–I(2)^{ii}	87.32(2)		
I(1)^{i}–Pb(1)–I(2)	87.32(2)		
I(3)^{iii}–Pb(1)–I(3)	93.542(13)		

$I(2)^{ii}$–Pb(1)–I(3)	90.52(2)		

Symmetry codes:(i) 1–x,1–y,1–z; (ii)+x,+y,1+z; (iii) 1/2+x,1/2–y,+z; (iv) +x,+y, –1+z; (v) –1/2+x,1/2–y, +z;

(Mpda)Pb_2I_6-298K

I(2)–Pb(1)–I(2)i	179.46(4)	Pb(1)–I(2)	3.2374(2)
I(3)–Pb(1)–I(2)	90.256(19)	$Pb(1)–I(2)^{i}$	3.2374(2)
$I(3)^{ii}$–Pb(1)–I(2)	90.06 (2)	Pb(1)–I(3)	3.1823(10)
$I(3)^{ii}$–Pb(1)–$I(2)^{i}$	90.07(2)	$Pb(1)–I(3)^{ii}$	3.2068(12)
I(3)–Pb(1)–$I(2)^{i}$	90.256(19)	$Pb(1)–I(1)^{iii}$	3.1846(10)
I(3)– Pb(1)–$I(3)^{ii}$	92.789(14)	Pb(1)–I(1)	3.2015(9)
I(3)–Pb(1)–I(1)	91.73(3)		
I(3)–Pb(1)–$I(1)^{iii}$	179.49(4)		
$I(1)^{iii}$– Pb(1)–I(2)	89.743(19)		
$I(1)^{iii}$–Pb(1)–$I(2)^{i}$	89.743(19)		
I(1)–Pb(1)–I(2)	89.91(2)		
I(1)–Pb(1)–$I(2)^{i}$	89.91(2)		
$I(1)^{iii}$–Pb(1)–$I(3)^{ii}$	87.72 (3)		
I(1)–Pb(1)–$I(3)^{ii}$	175.48(3)		
I(1)–Pb(1)–$I(1)^{iii}$	87.76(3)		
Pb(1)–I(2)–$Pb(1)^{iv}$	179.46(4)		
Pb(1)–I(3)–$Pb(1)^{v}$	151.34(5)		
Pb(1)–I(1)–$Pb(1)^{iii}$	92.24(3)		

Symmetry codes:(i)+x,+y,1+z; (ii) –1/2+x, 3/2-y,+z; (iii) 1–x, 1–y, 2–z; (iv) +x, +y, –1+z; (v) 1/2+x,3/2–y, +z;

(H_2bda)Pb_2I_6-298K

$Pb(1)^{i}$ –I(1)–Pb(1)	92.34 (2)	$Pb(1)^{i}$ –I(1)	3.1222(8)
$Pb(1)^{ii}$–I(2)–Pb(1)	149.27(3)	Pb(1)–I(1)	3.1899(9)
Pb(1)–I(3)–$Pb(1)^{iii}$	176.34(4)	$Pb(1)^{ii}$–I(2)	3.1820(9)
$I(1)^{i}$–Pb(1)–I(1)	87.66(2)	Pb(1)–I(2)	3.2355(9)
$I(1)^{i}$–Pb(1)–I(2)	177.03(3)	Pb(1)–I(3)	3.2007(8)
$I(1)^{i}$– Pb(1)–$I(2)^{iv}$	87.10(2)	$Pb(1)^{iii}$–I(3)	3.3092(8)
$I(1)^{ii}$–Pb(1)–I(2)	89.52(2)		
I(1)–Pb(1)–$I(3)^{v}$	87.19(2)		
I(1)– Pb(1)–I(3)	96.44(2)		
$I(1)^{ii}$–Pb(1)–I(3)	90.46 (2)		
$I(1)^{ii}$–Pb(1)–$I(3)^{v}$	90.12(2)		
$I(2)^{iv}$ –Pb(1)–I(1)	170.62(2)		
$I(2)^{iv}$ –Pb(1)–I(2)	95.823(15)		
$I(2)^{iv}$ –Pb(1)–$I(3)^{iii}$	85.04(2)		
$I(2)^{iv}$–Pb(1)–$I(3)^{ii}$	91.37(3)		
I(2)–Pb(1)–$I(3)^{v}$	90.67(2)		

I(3)–Pb(1)–I(2)	88.94(2)
I(3)–Pb(1)–I(3)^{v}	176.34(4)

Symmetry codes:(i) 1–x,1–y,2–z; (ii) +x, 1/2–y, –1/2+z; (iii) 1+x,+y,+z; (iv) +x, 1/2–y, 1/2+z; (v) –1+x, +y, +z

Table S4. Survey of intra-octahedral distortions in $(M_2pda)Pb_2I_6$.

Distortions parameters	Intraoctahderal distortions	
	Δd ($\times 10^{-4}$)	σ^2 ($^{\circ 2}$)
$(M_2pda)Pb_2I_6$ (LTP)	6.1	7.3
$(M_2pda)Pb_2I_6$ (HTP)	0.9	5.9

Note (see Fig. S7):

Intraoctahedral distortions within a single PbI_6 octahedron are quantified by bond length distortion Δd:

$$\Delta d = (\frac{1}{6})\Sigma\frac{(d_i - d_o)^2}{do^2}$$

where d_i denotes the six Pb–I bond lengths and d_o is the mean Pb–I bond length, and bond angle variance σ^2:

$$\sigma^2 = (\frac{1}{11})\sum_{i=1}^{12}(\theta_i - 90)^2$$

where θ_i denotes the individual I-Pb-I bond angles.

Table S5. Structure optimization for DFT calculation.

		a	*b*	*c*	*β*	*volume*	Err%
$(M_2pda)Pb_2I_6$	exp	9.13480	17.66630	6.42660	90	1037.112590	
	PBE	9.24881	17.22519	6.37258	90	1015.231737	–2.11